On the use of process analytical technologies and population balance equations for the estimation of crystallization kinetics. A case study.

Nesrine Gherras, Gilles Févotte

On the Use of Process Analytical Technologies (PAT) and Population Balance Equations for the Estimation of Crystallization Kinetics. A Case Study.

GHERRAS Nesrine[a], FEVOTTE Gilles[a,b*]

[a] Ecole des Mines de Saint Etienne, centre SPIN, LPMG, UMR CNRS 5148.

158, cours Fauriel. 42000 Saint Etienne (France)

[b] Université de Lyon, Université Lyon 1, 43 bld du 11 Novembre 1918. 69100 Villeurbanne (France)

Abstract

The batch cooling solution crystallization of Ammonium Oxalate (AO) was performed in water at various constant cooling rates. Measurements of the solute concentration were obtained using *in situ* ATR FTIR spectroscopy, and discrete-time estimates of the Crystal Size Distribution (CSD) were computed thanks to *in situ* image acquisition and off-line image analysis. The crystallization process was then simulated using Population Balance Equations (PBE). Estimates of the nucleation and growth parameters were computed through model/experiments fitting. According to the cooling rate, the PBE model allowed distinguishing between two distinct crystallization regimes, separated by an "intermediate regime".

The results allow assessing the respective contributions and shortcomings of solute concentration measurements and granulometric data to the identification of nucleation and growth kinetic parameters. It is shown in particular that no real separate estimation of nucleation and growth parameters can be obtained in the absence of CSD data.

Corresponding author : gherras@emse.fr; fevotte@emse.fr

Introduction

Batch crystallization is extensively used in chemical and pharmaceutical industry as a separation and purification process, especially when small scale production of high value added chemicals is concerned. The control of batch crystallization process is essentially intended to improve the CSD with respect to the processing properties of the particles, the purity of final crystals and the crystal habits and morphology. Indeed, controlling these properties remains a important industrial issue since most particle features influence the ease of processing of the final product (e.g. flowability, filterability, caking or dusting ability) and many of its quality and end-use properties (e.g. dissolution rates, apparent density, hardness, specific area, etc.) To a large extent these latter properties also depend on the bulk properties of the solid such as defect content (e.g. structure dislocation, solvent occlusions, etc.) and chemical purity. Consequently, there is a clear need to better understand how operating parameters like solvent, supersaturation and temperature profiles, impurities, hydrodynamics, etc. can affect the final product properties. Indeed, the question of manipulating such process variables in order to control the bulk and surface properties of materials is of tremendous importance.

During the last fifteen year, the significant development of in situ on line measurement techniques for monitoring crystallization processes allowed many progresses regarding the control of both the quality and reproducibility of particulate products[1-3]. In the field of pharmaceutical development and production, the `PAT' initiative of the FDA [1,4] is a good illustration of the expectations and successes associated to a better control of industrial crystallizers. From a more academic point of view, continuous and *in situ* measurement tools made it possible to obtain refined experimental results and allowed advanced modeling and control approaches to be developed. Former approaches were indeed usually using infrequent off-line suspension samples: sampling and analyzing crystallizing suspensions remains a complex and poorly reliable method which is also limited by the restricted number of possible measurements.

Many innovative applications of PATs to the advanced dynamic modeling and control strategies to crystallization processes are described in the literature. The results of these studies can be implemented in the industrial context thanks to PATs. Among recent modeling and/or control studies one can mention modeling and monitoring of phase transitions processes [5,6], of optical isomer separation processes [7], of crystal shape evolutions [8-10], agglomeration and attrition phenomena [11-15], etc. Of course, PATs offer tools

for the design and development of advanced feedback control strategies requiring the development of dynamic crystallization models. As far as identifying the related kinetics models is concerned, it is clear that many parameters have to be identified. Unfortunately, the relevance and the significance of parameter estimation techniques in the mathematical framework of highly nonlinear, non stationary and coupled phenomena such as nucleation, crystal growth or agglomeration remain questionable. Few studies were actually devoted to this question (see e.g. [16-18]). Despite the importance of the problem of parameter sensitivity and "identifiability" many authors still have recourse to old and relatively rough methods for estimating nucleation parameters, which theoretical bases are questionable. For example, measurements of induction times and metastable zone width aiming at evaluating the kinetics of nucleation remain largely practiced [19-21] To some extent, the present study brings these latter methods into question and, from a practical point of view, aims at addressing the following question: as far as in line sensors could be made available for kinetic parameters identification purposes, is it essential, or not, to use information on both liquid and dispersed solid phases in presence?

Ammonium Oxalate (AO) monohydrate dissolved in water was here selected as a model-system. Previous workers have thoroughly reviewed the crystallization of AO [22-24]. The mechanisms and kinetics of crystal growth and nucleation were studied, and the effect of some cationic impurities on the nucleation and growth processes was also investigated [25-28] However, the published models are always derived from specific experiments assuming the separation of crystal nucleation and crystal growth so that the corresponding rates are usually estimated from single crystals experiments at fixed temperature and/or supersaturation [23]. Moreover, in many cases, the nucleation parameters are characterized by induction time or metastable zone width measurement methods [29,22]. Due to their simplicity and to the very restrictive hypotheses made, these latter methods present weaknesses and approximations which justify their call into question.

In this paper the nucleation and growth characteristics of ammonium oxalate crystals produced during batch cooling crystallization operated at different cooling rates are investigated to illustrate the subject. Indeed, advanced model based design approaches require accurate kinetics and thermodynamic data which are not always easy to determine This work is therefore focused on the development of experimental and numerical protocols for the estimation of nucleation and growth kinetics, as well as on the development of suitable models for process development and optimization purposes.

During the present study *in situ* image acquisition and ATR-FTIR spectroscopy were used for real time process monitoring. Models describing the dynamic behavior of the crystallization process were designed thanks to the mathematical framework of Population Balance Equations (PBE). The nucleation and growth kinetic parameters were then estimated using "standard" non-linear numerical optimization techniques (i.e. through the minimization of quadratic criteria quantifying the difference between the experimental data and the model-predicted ones.)

Population balance equations

Population Balances Equations (PBEs) are widely used as a mathematical framework in the engineering of dispersed media, with applications including crystallization, powder technologies, polymerization processes, biotechnologies, etc (see e.g.[30-33]).

Crystal growth rate

In the field of crystallization, most published PBE modeling works assume that the crystal growth rate *G* does not to depend on the particle size (McCabe's hypothesis), but essentially on supersaturation. Several expressions of supersaturation may be defined, according to the theoretical background of the study. The following equations define both the relative supersaturation σ(t) and the supersaturation ratio *β(t)*, which both are adimensional variables used in kinetic models:

$$\sigma(t) = \frac{C(t) - C^*(T)}{C^*(T)} \quad (1)$$

$$\beta(t) = \frac{C(t)}{C^*(T)} \quad (2)$$

The following expression can also be used as an expression of the crystallization driving force:

$$\Delta C(t) = C(t) - C^*(T) \quad (3)$$

C* is the equilibrium concentration (i.e. the solubility of the solid crystallizing compound in a given solvent) and C(t) is the solute concentration.

The growth of crystals from solution is a complex process. Depending on the solute-solvent system in question, many steps may be involved during the crystal growth (e.g. bulk and surface diffusion, solvation, integration, etc) and this is the reason why "standard" models used to represent the growth process are

more or less comprehensive and approximate (see e.g.[34-36]). The crystal growth rate is usually approximated as the rate at which a specific or an average characteristic size *L* of crystals increases:

$$G(t) = \frac{dL}{dt} \tag{4}$$

Many expressions of the growth rates were formulated. For example, the celebrated BCF (Burton, Cabrera and Franck) screw dislocation model was proposed in 1951 [37]. The following expression is rather versatile as it can be used to represent various growth mechanisms, according to appropriate parameters c and D:

$$G_{BCF}(t) = \frac{dL}{dt} = c\frac{(\beta(t)-1)^2}{D}\tanh\left[\frac{D}{\beta(t)-1}\right] \tag{5}$$

The BCF model roughly corresponds to the following orders of supersaturation dependency:

$G \propto \sigma^2$ for low values of σ and $\exists \sigma_c$ with $G \propto \sigma$ for $\sigma > \sigma_c$ (6)

Experimental results about the linear growth rates of ammonium oxalate monohydrate [$(NH_4)_2C_2O_4 \cdot H_2O$; AO] single crystals have been published by Mielniczek-Brzóska and Sangwal [38]. The crystals were grown through constant-temperature or constant-supersaturation processes at 30 and 40 °C in the supersaturation range of 1–9%. The supersaturation dependence of the growth rate was reported to obey a parabolic growth law.

First principle models like Eq. (5) should not necessarily be used for process engineering applications. Due to their simplicity and to the limited number of parameters involved, basic phenomenological models are currently applied, despite their lack of physical meaning. Such models usually assume power supersaturation dependency of the growth rate as follows:

$$G(t) = k_g \sigma(t)^j \tag{7}$$

where exponent *j* depends on the involved growth mechanism(s) which, in particular, is known to depend on the level of supersaturation. In practice, consistently with "standard" theoretical models, most published values of *j* are given between 1 and 2. k_g is a temperature-dependent growth parameter.

Crystal nucleation rate

Many primary and secondary nucleation models are available in the literature. The following expression of primary homogeneous nucleation is derived from the Classical Nucleation Theory (CNT). This latter model will be used here to simulate primary homogeneous nucleation occurring during batch unseeded cooling crystallization of AO:

$$R_{N_1}(t) = A_{\text{hom}} \exp\left[\frac{-B_{\text{hom}}}{T^3 (Ln\beta)^2}\right] \quad (8)$$

Theoretical expressions of parameters *A* and *B* can be found in the literature, see e.g. [34,39]. According to the theory of homogeneous nucleation the following expressions are typically used, according to the mechanism in question:

$$B_{\text{hom}} = \frac{16\pi \nu_0^{\,2} \gamma^3}{3(kT)^3} \quad (9)$$

$$\mathrm{A_{hom,D}} = \mathcal{D}\left[\frac{\mathrm{kT}}{\nu_0^{\,2}\gamma}\right]^{1/2} \mathcal{N}_{\mathrm{A}} \mathrm{C}^* \ln\beta \quad (10)$$

Eq.(10) corresponds to diffusion controlled nucleation while the following expression is used to describe nucleation controlled by interface transfer :

$$A_{\text{hom},I} = \mathcal{D}\left[\frac{\gamma}{kT}\right]^{1/2}\left[\frac{4\pi}{3\nu_0}\right]^{1/3} \mathcal{N}_A \mathrm{C}^* \quad (11)$$

When heterogeneous nucleation is the predominant mechanism, parameter *B* is given by the following expression:

$$B_{het} = \mathcal{D}\frac{16\pi \nu_0^2 \gamma_{eff}^3}{3(kT)^3} \quad (12)$$

Where *T* is the absolute temperature (K), $\mathcal{D}$ is the diffusivity of the solute ($m^2.s^{-1}$), ν_0 is the solute molecular volume, γ is the crystal-liquid interfacial energy ($J.m^{-2}$) and k is the Boltzmann constant ($J.K^{-1}$).

Expressions (9) and (12) differ in the value of the interfacial energy: when heterogeneous nucleation takes place, γ is replaced by γ_{eff} , which is usually significantly smaller.

Secondary nucleation was found to take place during the crystallization of ammonium oxalate. This latter mechanism appeared to be promoted by increasing amounts of solid in suspension. Numerous phenomena can be referred to as secondary nucleation (initial breeding, attrition, etc.), which were the object of intense researches during the past decades [39,35,40]. However the many related elaborated models cannot always easily be identified. Moreover, several secondary mechanisms are likely to occur simultaneously. For the sake of simplicity, secondary nucleation phenomena is therefore represented below using a phenomenological kinetic equation accounting for the dependence of secondary nucleation rate upon $\sigma(t)$, the energy dispersed through agitation ε_a and the concentration of solid in suspension $C_S(t)$:

$$R_{N_2}(t) = A_{SN}\ C_s(t)^k\ \sigma(t)^i\ \varepsilon_a{}^n \tag{13}$$

In order not to increase unreasonably the number of estimated parameters, A_{SN} was considered constant in the range of experimental temperature used in this study. Exponent *k* and *i* are commonly found between 0 and 2. The input stirring power will not be considered in this work since the stirring rate was kept constant during the experiments.

Monodimensional PBEs modelling of the cooling crystallization process.

Computing the supersaturation ratio β(t) requires measurements of the solute concentration C(t) during the crystallization process. During the batch process, the decrease of C(t) is obviously caused by the generation of crystals since the molecules of solute initially present in the liquid phase are transferred through crystallization to the dispersed solid phase. The total amount of solid is therefore given by the total volume of particles computed through the integration of the whole CSD:

$$C_s(t) = \frac{\rho_s \varphi_p}{M_s} \int_{L^*}^{\infty} \psi(L,t) L^3 dL \cong \frac{\rho_s \varphi_p}{M_s} \int_{0}^{\infty} \psi(L,t) L^3 dL \tag{14}$$

where ρ_s (kg/m^3) and M_s are the density and the molecular weight of the solid compound, φ_p is a volumetric crystal shape factor (e.g. π/6 in the "ideal" case of spherical crystals and π/25 for the anisotropic particles involved in the following.)

Eq.(14) allows computing C(t) at each time step and thus yields β(t) through Eq.(2), provided that experimental data about the solubility curve C*(T) are available. In the following, the crystallization is assumed to take place in a perfectly mixed batch reactor, new crystals are assumed to be generated through nucleation phenomena only and according to the CNT, the size of new particles generated in the dispersed phase is the critical size L^*, which is neglected below (i.e., from a purely numerical viewpoint). Moreover, agglomeration or breakage phenomena are neglected in the sequel.

Perfect mixing of the suspension implies that the number density function does not depend on external space coordinates. The following boundary conditions link the nucleation rate(s) of crystals to the overall particle number. In the case of mono-dimensional particles, the previous assumptions lead to the following

PDE describing the time variations of the Crystal Size Distribution (CSD), where $\psi(L,t)$ is the number population density function of crystals of size L, at time t:

$$\frac{\partial \psi(L,t)}{\partial t} + G(t)\frac{\partial \psi(L,t)}{\partial L} = 0 \quad (15)$$

$$\psi(L,0) = 0 \quad (16)$$

$$\psi(0,t) \approx \psi(L^*,t) \approx \frac{R_N(t)}{G(t)} \quad \perp \quad (17)$$

$R_N(t)$ is the overall rate of nucleation expressed in $\#.s^{-1}.m^{-3}$ (i.e., the sum of primary and secondary nucleation phenomena).

A simplified method of characteristics (MOC) was applied during the present study to solve numerically the PBEs [41]. The low computation time of the method appeared valuable for further use of non-linear optimization techniques required by the estimation of kinetic parameters.

Parameter identification of the crystallization kinetic parameters.

It is obvious that, as far as quantitative kinetic crystallization studies are concerned, the experimental data should provide enough information to enable the evaluation of several simultaneous and coupled phenomena. In practice, it is very difficult to "isolate" these latter phenomena (i.e., to make specific observations of every single phenomenon such as homogeneous or heterogeneous nucleation and growth), or at least to separate their respective contribution to the overall crystallization process. An example of this difficulty is given below where it is shown that even accurate measurements of the time variations of solute concentration do not allow estimating the nucleation rate. This shortcoming arises from the fact that experimental CSD data are essential to make the distinction between nucleation and growth effects in the overall solute consumption.

Now, assuming that appropriate data describing both the dispersed and the continuous phase are available, estimates of the parameter values can be obtained through the minimization of the discrepancy between experimental data and model predictions. The optimization procedure used in the following is based on the following weighted non linear quadratic criterion:

$$J(t,n,\underline{\theta}) = \min\left(\sum_{n=1}^{N_{\exp}} \left[\frac{1}{t_{n,end}} \int_{t=0}^{t_{n,end}} \left[\tilde{C}_n(t,\underline{\theta}) - \hat{C}_n(t) \right]^2 dt + \lambda \sum_{k=0}^{k_{\max}} \left[\tilde{\varphi}_k(L_k,\underline{\theta}) - \hat{\varphi}_k(L_k) \right]^2 \right] \right) \quad (18)$$

with $\underline{\theta} = \left[k_g\,,\ A_{\text{hom}}\,,\ B_{\text{hom}}\right]$ (19)

where $n \in [0, N_{exp}]$ refers to one given experiment used for the estimation of the vector of parameters $\underline{\theta}$ (N_{exp} experiments are gathered in the estimation procedure) ; $t_{n,end}$ is the duration of the n^{th} experiment ; k is the number of a given class of particle size ($k \in [0, k_{max}]$) ; φ_k is the number of particles belonging to the class of average size L_k and λ is a weighting factor introduced to balance the influence of the two variables (i.e. the "almost continuous" concentration profile and the discretized size distribution histograms) determining the final optimal value of $J(\theta)$. In practice, λ was set empirically such that *a posteriori* plots of the model/experiments supersaturation and final CSD profiles appeared satisfactory. Moreover, notations ^ and ~ refer to the measured and model-predicted variables, respectively.

The optimization problem was solved using *lsqnonlin* from the MATLAB® optimization toolbox. Figure 1 displays a schematic of the whole numerical parameter estimation procedure.

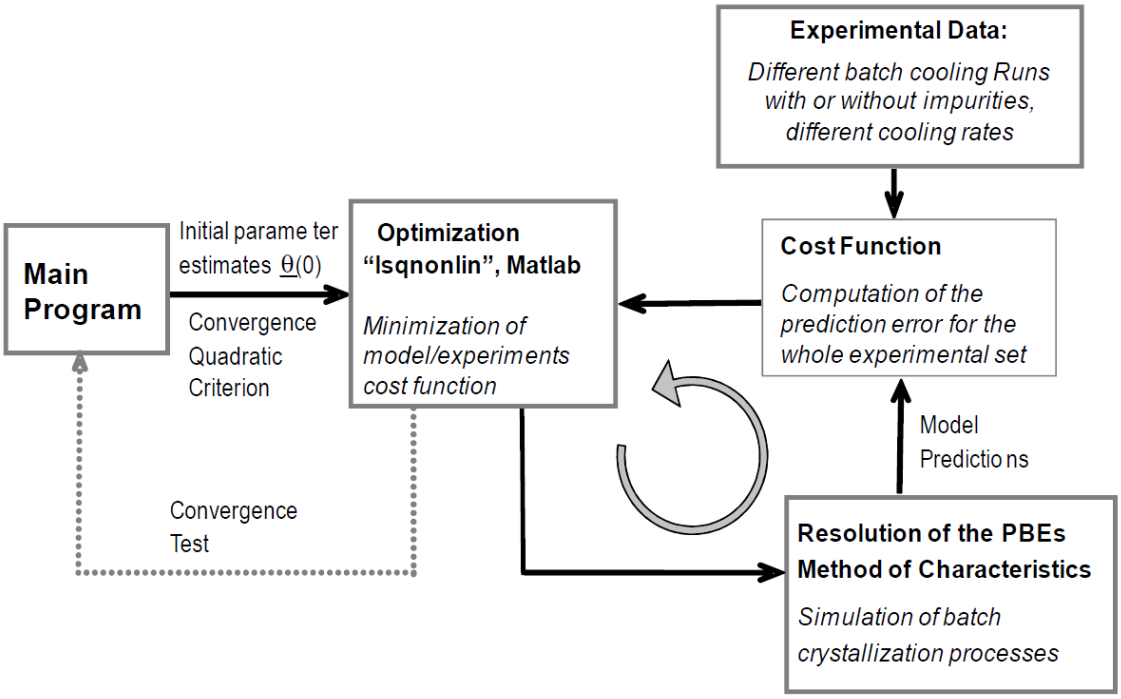

Figure 1. Schematic of the identification procedure for the estimation of the nucleation and growth kinetic parameters $\underline{\theta}$ of AO batch cooling crystallization.

Experimental

Materials

As already mentioned, Ammonium Oxalate (AO) monohydrate was used as model product in the crystallization experiments. AO was available from Acros Organics with a purity level of 99+%. The product was used as received, without further purification. Distilled, de-ionized and degassed water was used as solvent.

Batch crystallizer set up and in situ characterization techniques

The experiments were performed in a 3 L glass vessel equipped with a jacket and a condenser. The jacket was baffled and a pump forced the circulation. Stainless–steel baffles and a high efficiency propeller (Mixel TT TM) were used to maintain a good homogeneity of particles in the slurry. The bench-scale plant was instrumented and computer-controlled to allow tracking set-point temperature trajectories. Cooling was performed by means of heat transfer through the jacket wall: the temperature was controlled by manipulating automatically the set-point temperature of a heating bath containing water and glycol with an accuracy of ± 0,5°C.

I*n situ* concentration measurements were acquired using the infrared spectrometer "MATRIX-F" manufactured by Brucker Optik GmbH, equipped with ATR-diamond immersion probe also manufactured by Brucker Corporation (diamond prism with two reflexion angles of 45°). The ATR probe was connected to the spectrometer through optical fiber. The measurement cell, the optical conduit and the probe were purged using nitrogen in order to avoid difficulties raised by the sensitivity of the measurements to the time variations of the concentration of water and carbon dioxide in the ambient air. The source of light is a polychromatic laser emitting in mid-IR. The detection is ensured by a MCT detector cooled with liquid nitrogen. The resolution of the detection was set to 4 cm^{-1}. The IR spectra were acquired with a sampling period of 30 seconds during which the calculation of an average spectrum was obtained from 32 scans. Measurements of solute concentration were presented in many papers and the principle of these measurements will not be recalled here [42-45]. In particular, calibration procedures were explained elsewhere[46]. After validation, the calibration model was firstly used to evaluate the time variations of supersaturation, as displayed in Fig.2. The solubility curve displayed in Figs. 4-6 was also obtained using continuous ATR FTIR measurements, as already presented in [47]: thanks to slow cooling and heating of AO suspensions, very low levels of super- and under-saturation can be covered such that the two measured

curves can be made as close as possible. The unique curve finally obtained or the average of the two curves is then assumed to fit the solubility [46].

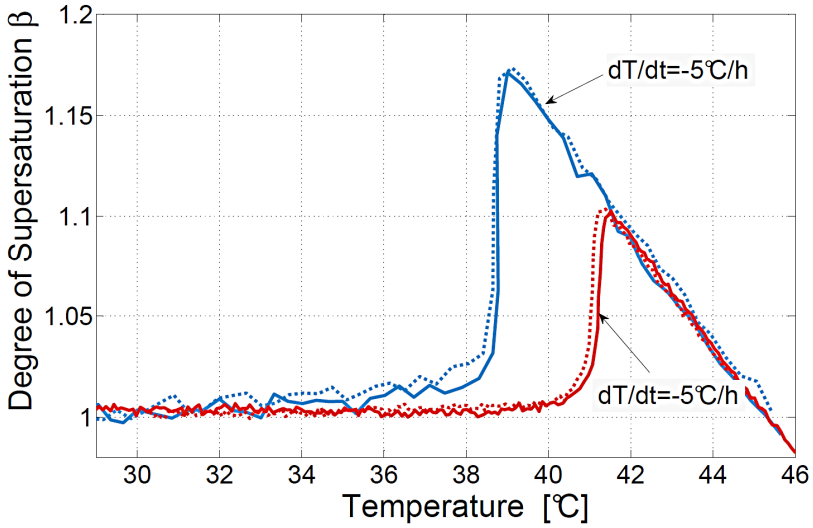

Fig.2: Supersaturation profiles measured during AO crystallization in water performed at two cooling rates (7°C/h & 20°C/h). The two sets of two runs show the reproducibility of the process and of the ATR FTIR measurements.

In addition to in situ FTIR measurement of solute concentration, the CSD of the final product was measured through image analysis, using the "EZProbe" [48], an in-situ imaging probe developed at the University Lyon 1. The imaging probe allowed real time acquisition of 2D images of AO particles during the batch process, as shown in Fig.3. Size measurements were then performed for each discernible crystal, with a minimum sample of 900 crystals per CSD analysis. Due to the time required by the processing of the video pictures, few CSD were actually evaluated for each experiment. toto

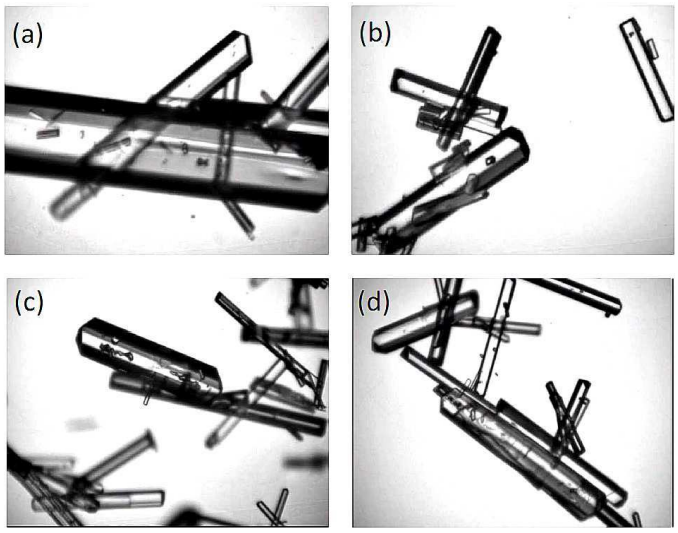

Experimental procedure for linear batch cooling experiments.

For the sake of industrial applicability the experimental design was focused on the joint investigation of the nucleation and growth kinetics of AO monohydrate during batch cooling runs. Seeding was not found to be necessary for the reproducibility of the experiments. As one can see in Figs.2, the onset of primary nucleation turned out to be satisfactorily reproducible.

AO undersaturated solutions were prepared by dissolving appropriate amounts of analytical grade ammonium oxalate monohydrate in 1800 ml water. The initial AO concentration was always 0.1 kg/kg solvent. In order to ensure complete dissolution, the suspensions were heated several degrees higher than the saturation temperature (323K) and maintained for at least 2 hours at this temperature. The completion of the dissolution was checked using both ATR-FTIR and image acquisition. Linear cooling experiments were then carried out at varying linear cooling rates, namely: 2, 5, 7, 10, 12, 20, 25 and 30 °C/h. for the sake of repeatability at least 3 experiments were performed for each cooling rate. Cooling was stopped at 293K and followed by a period of stabilization of 3 hours at this latter temperature. Suspension samples were then withdrawn at 293K, filtered off and dried for optical microscopy and SEM investigation.

Parameter estimation and simulation results:

Some questions about estimating crystallization parameters using concentration measurements only.

Figure 2 shows the "measured" supersaturation profiles obtained during the batch cooling crystallization of AO in water at two different cooling rates (-7°C/h & -20°C/h). As expected, increasing cooling rates widen the apparent metastable zone width and increase the maximum relative supersaturation (see also Fig.6).

As above outlined, a major question is raised concerning the relevancy of studies devoted to the kinetic estimation and modelling of crystallization processes when no CSD data (even average or partial experimental data about the dispersed phase) is made available. Is it realistic to expect even a rough estimation of both nucleation and growth kinetic parameters from solute concentration measurements only? As a first answer to this question, one can argue that many slowly growing particles (i.e. high nucleation rate can occur together with slow growth rate) could lead to the same solid consumption than few rapidly growing particles. Therefore, identical concentration trajectories could be simulated using different sets of kinetic parameters and yield different final simulated CSD profiles.

Actually, it is clear that there is a one-to-one relationship between the supersaturated concentration point where the concentration starts to decrease during a given batch cooling process, and the value of parameter B_{hom}. Nucleation and growth models can only be fitted thanks to a single value of B_{hom} because the experimental limit of metastable zone clearly corresponds to a unique value of B_{hom}. Moreover, during the present study, it was observed that the "best" PBE simulation of the experimental concentration trajectory, obtained after minimization of the model vs. experimental concentration mismatch predicts excessively small particle sizes. To illustrate this point, Fig.4a displays an exact fit obtained between the measured and simulated solute concentration profiles for dT/dt=-10°C/h, and it makes no doubt that the simulation "predicts" unrealistic final particle size of the order of 10-20 μm (i.e., in Fig.4c the final average particle size is 10 μm), while *in situ* measurements obtained thanks to the EZProbe show much bigger particles (i.e., about hundred times larger.)

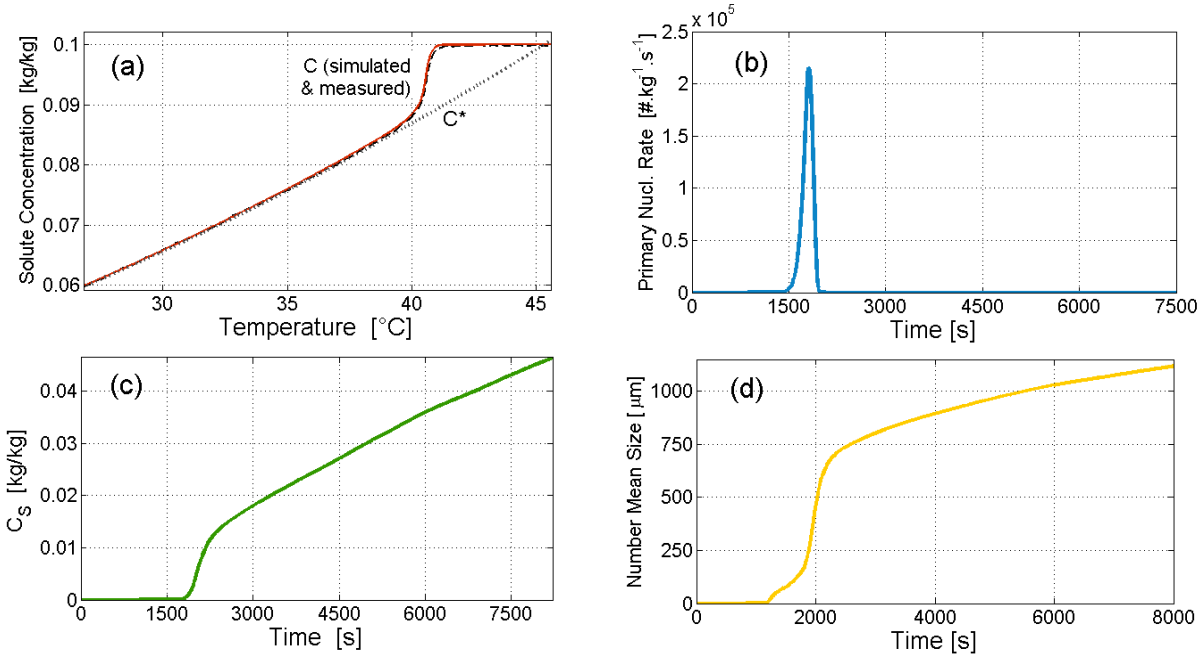

Figure 4

It turns out that there exists an infinity of "optimal" binomials (A_{hom}, k_g) leading to the exact representation of a given supersaturation profile. This feature is illustrated in Fig.5 where the simulation results are displayed for 3 different values of parameter A_{hom}. Setting any value of A_{hom} appears to be compatible with the exact fit of solute and solids experimental concentration profiles. Indeed, Fig. 5 displays 3 perfectly superimposed simulated and experimental C(t) curves where decreasing values of A_{hom} are combined with increasing values of the growth rate constant k_g (curves 1 till 3 in Fig.5b and 5d),

In order to shed some light on the connection between A_{hom} and k_g , Appendix A demonstrates that an "exact" fit of the measured concentration trajectory is obtained for a single product $A_{hom}.k_g^3$, whatever the value of A_{hom} , when the crystallization process is assumed to be initiated through primary nucleation only (i.e., Eq.(8) is assumed to represent the entire nucleation process). Consequently, without additional information on the real particles sizes, nucleation and growth kinetics remain "intricate". Roughly speaking, the solute concentration data does not "contain" enough information about the mechanisms responsible for the generation of new particles over time. In addition to accurate experimental measurement of the solute concentration, information about the "true" particle size is therefore required. The optimization results presented in Fig. 5 strengthen and clarify the idea that no identification of the pre-

exponential parameter of the primary nucleation rate is made possible without CSD

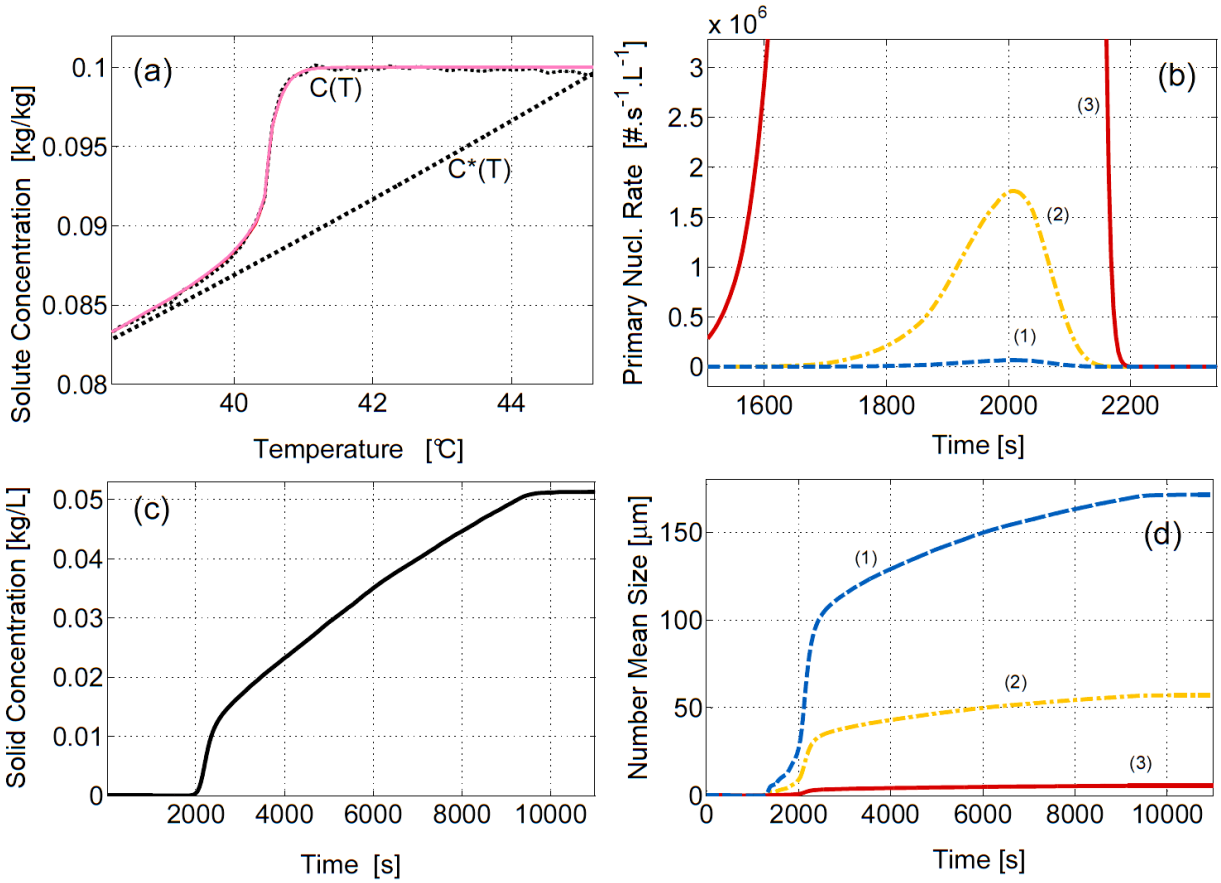

Figure 5

As far as induction time techniques are concerned, it follows that since these methods do not account for any information about growth rates or CSD (except very vague assumptions about the amount and/or the size of solid particles observed when the metastable zone limit is supposed to be reached) one cannot expect relevant estimation of the nucleation rate to be obtained.

It can also be concluded from Fig.5 and Appendix A that during the parameter optimization procedure, setting any *a priori* value of parameter k_g will not keep the algorithm to converge towards a single "optimal" value of product $A.k_g^3$. In the absence of additional experimental information, k_g was therefore set to 2.10^{-5} m/s in the following. This value was selected such that the final maximum particle sizes (the size of particles born at the beginning of the crystallization process) roughly correspond to the observed ones.

Crystallization parameter estimation based on experimental solute concentration profiles.

Fig. 6 presents the experimental and computed time variations of solute concentration profiles for 6 runs performed with varying cooling rates. The simulated results were obtained as explained above. Here, the optimization was only based on the ATR FTIR *in situ* concentration measurements. At low cooling rates, the simulated concentration profiles satisfactorily fit the experimental data and it should be noted that the phenomenological Eq.(7), did not call for particular refinement. For example, reproducing the overall dynamics of the process did not require accounting for the effect of temperature on the growth kinetic constant k_g. The related estimated kinetic parameters are given in Table 1.

It is also interesting to note that without CSD data the parameter optimization procedure predicts negligible secondary nucleation as an additional mechanism for the continuous generation of new particles during slow cooling batch operations. In this latter case, which will be referred to as regime R_1 in the following, introducing Eq.(13) in addition to the nucleation kinetic expression (8) turned out to be useless and did not allow improving the fit between the experimental and the simulated results. Figure 4 displays an example of accurate fit between the model and the experiments, obtained with $B_{het}= 0$ for a cooling rate of -10°C/h. The related predicted nucleation profile also presented in Fig.4b, this peak is rather narrow and no significant rate of secondary nucleation was found to improve the model predictions.

It is worthy of noting that the crystallization regime R_1 was satisfactorily described using the same set of primary homogeneous nucleation parameters. The single set of kinetic parameters was obtained using (up to 4) model/experiments data sets were used simultaneously to feed the optimisation procedure. Regime R_1 was found to occur for cooling rates between -2° and -12°C/h. The corresponding model is referred to as "Model 1" in Table 1, the simulated C(t) variations are displayed in both Figs. 6 and 7.

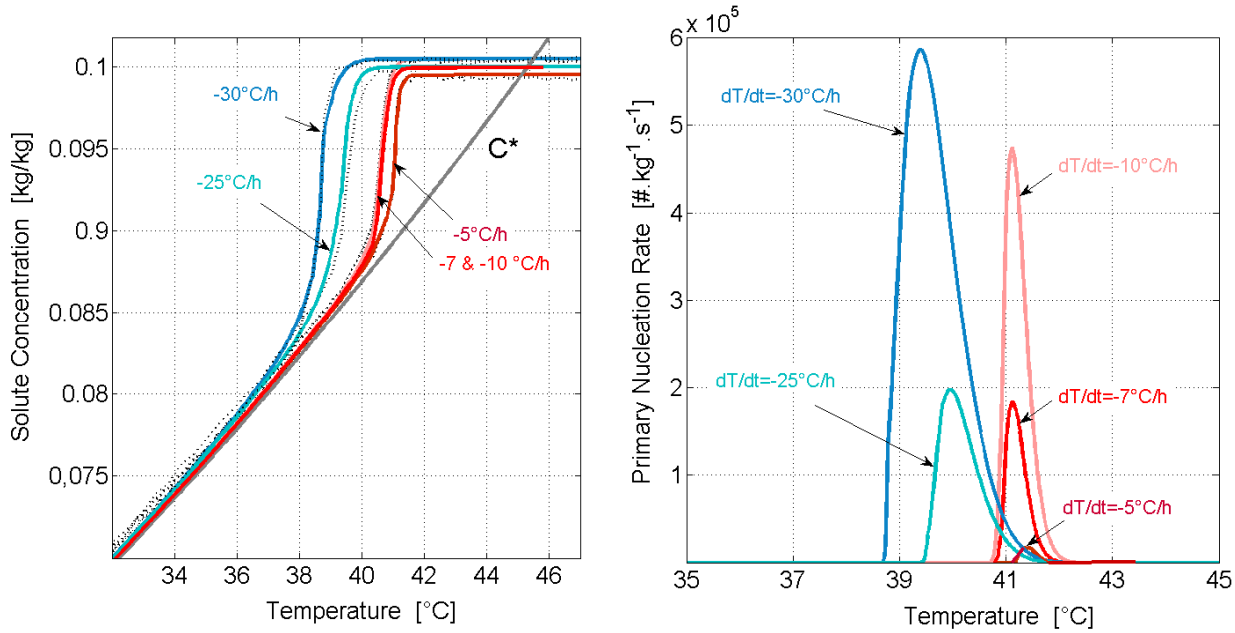

Figure 6

In contrast to regime R_1, the application of an optimal set of nucleation and growth parameters to the simulation of the second crystallization regime R_2, is not really satisfactory (The model predictions are referred to as Model 2.1 in Fig.6 and Table 1) The results given by "Model 1" were obtained with optimal parameters computed from 4 experiments performed between -25 and -30°C/h. The plot of Model 2.1 for dT/dt=-30°C/h shows a rather poor fit between the model predictions and the solute concentration measurements. However, the separate optimization of the concentration profiles obtained at constant given cooling rate yields again a very satisfactory description of the solute consumption. The simulated concentration profile (Simul 2) obtained after fitting the experimental data obtained from two reproducible experiments performed at dT/dt=-30°C/h, is referred to as "Model 2.2". The corresponding parameters are also given in Table 1 and, as shown in Fig.6, the simulation based on these latter parameters fits exactly the measurements obtained during the experiments performed with a cooling rate of -30°C/h.

The modelling difficulties encountered in the case of regime R_2 allow concluding that crystallization of AO at "high" cooling rates involves more complex solid generation mechanisms than regime R_1. In order to better understand the observed differences between R_1 and R_2, the nucleation model for R_2 was assumed to result of primary homogeneous mechanisms triggering the generation of first particles, followed by secondary contact nucleation. Eq. (13) was therefore introduced in the computation of Eq.(17) giving the

overall rate of nucleation R_N. It finally turned out that accounting for secondary nucleation mechanisms in the modelling of regime R_2 allowed to fit the whole set of experimental data with a much better accuracy than previously. Figure 7 displays the experimental and simulated supersaturation profiles obtained for both regimes R_1 and R_2 using the set of optimal parameters given in Table 1 (i.e. Model 2.3) with secondary nucleation (i.e. $A_{SN} \neq 0$). Again, it appeared that the batch operations performed in the "intermediate regime" with dT/dt=-20°C/h were poorly described by the model as well all the experiments performed between -25 and -12°C/h (not presented here.) For these latter experiments no satisfactory modelling has been possible, due to the lack of reproducibility of primary nucleation phenomena.

Figure 8 is representative of the simulation results obtained with the parameters given in Table 1 (model 1 for R_1 and model 2.3 for R_2). The supersaturation profiles are satisfactorily reproduced by the model (Fig. 7) and Fig.8a and b show the simulated time variations of primary nucleation and secondary nucleation. The difference between the two regimes is clearly underlined by these results which show significant differences between the time variations of the nucleation rates and the dominating nucleation processes.

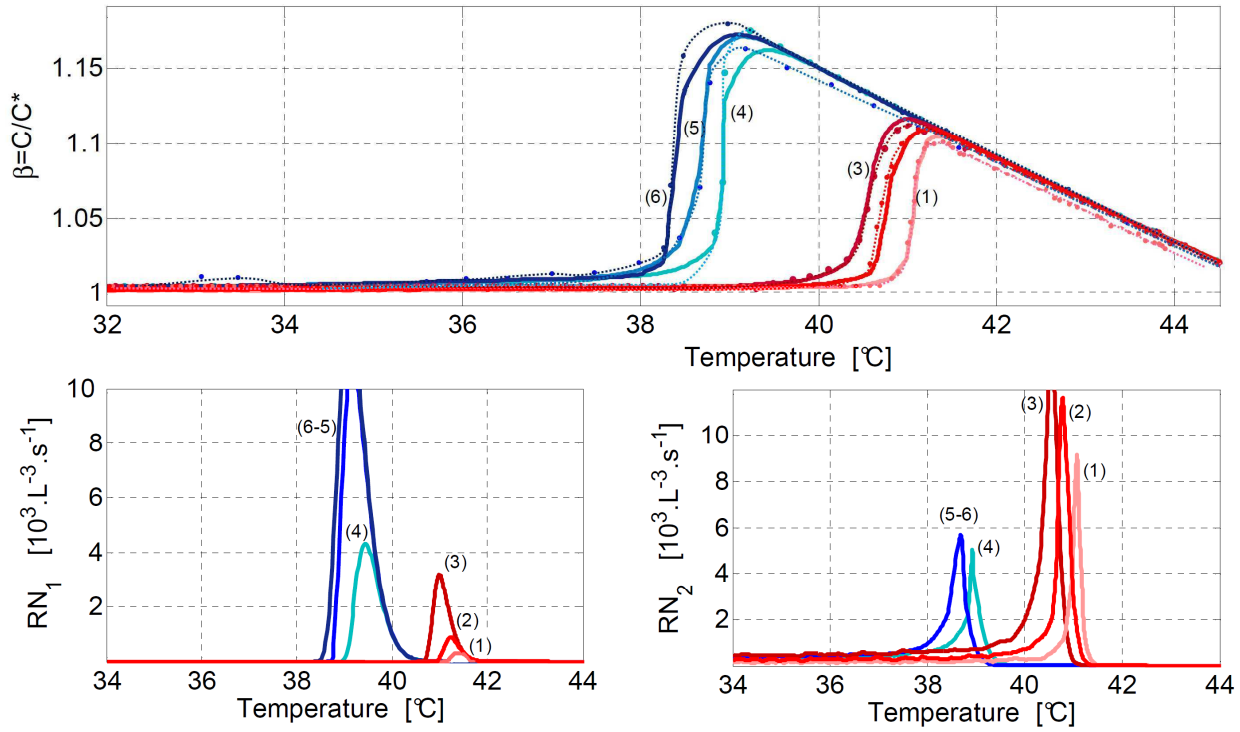

Figure 7-8

Fig. 7. Simulated and experimental relative supersaturation profiles σ(t) during regimes R_1 and R_2. The kinetic parameters for R_2 were computed without accounting for CSD data (model 2.3 in Table 1) and the parameters given in Table 2 were used to simulate R_1.

Fig.8. Simulation of the time variations of primary and secondary nucleation rates related to the data in Fig.7.

Crystallization parameter estimation based on both experimental solute concentration profiles and CSD data.

As above mentioned, the CSD of the growing particles was assessed using image analysis of the video pictures acquired during the crystallization experiments. Two examples of measured CSD corresponding to cooling crystallization processes performed at low and high cooling rates are displayed in Fig.9 and typical pictures of the growing crystals in suspension were shown in Fig.2. In the previous part dealing with the study of the nucleation mechanisms, only indirect and delayed information about the CSD was accounted for (i.e. Solute concentration measurements). Modelling the process led us to the hypothesis that secondary nucleation was perhaps negligible during regime R_1 while it appeared as prevailing during R_2. Now, a close observation of figures 2a-b and 2c-d, does not clearly allow concluding that a major difference in the nucleation mechanisms exists between R_1 and R_2. At first glance, in contradiction with the previous modelling observations, Fig.2 shows that the fines content, the overall crystal shapes and the "quality" of the crystal surfaces are not so different between the two regimes which were above highlighted. This is the reason why one could expect a more thorough experimental study accounting for data characterizing the time variations of the particles in suspension, to "soften" the kinetic data summarized in Table 1 and to put into perspective the previous observations about the weakness of secondary nucleation in regime R_1.

Now, the solute concentration measurements together with CSD data were taken into account for the minimization of criterion (14). The related estimated parameters are presented in Table 2. In contradiction to the previous approach, it clearly turned out that no satisfactory fit between the sets of experimental and simulated data could be obtained assuming a single primary nucleation mechanism, even for the crystallization regime R_1. The introduction of secondary nucleation in the model was the only way of explaining the spreading of the measured CSD. When CSD data are used in the optimization procedure, the accuracy of the model predicted supersaturation trajectory is slightly reduced, compared to the previous approach, but realistic particle sizes can now be represented thanks to the assumption of prevailing secondary nucleation. Typical simulation results are displayed in Fig.9 and 10 where two experiments performed with different cooling rate (-5 and -10°C/h) are shown.

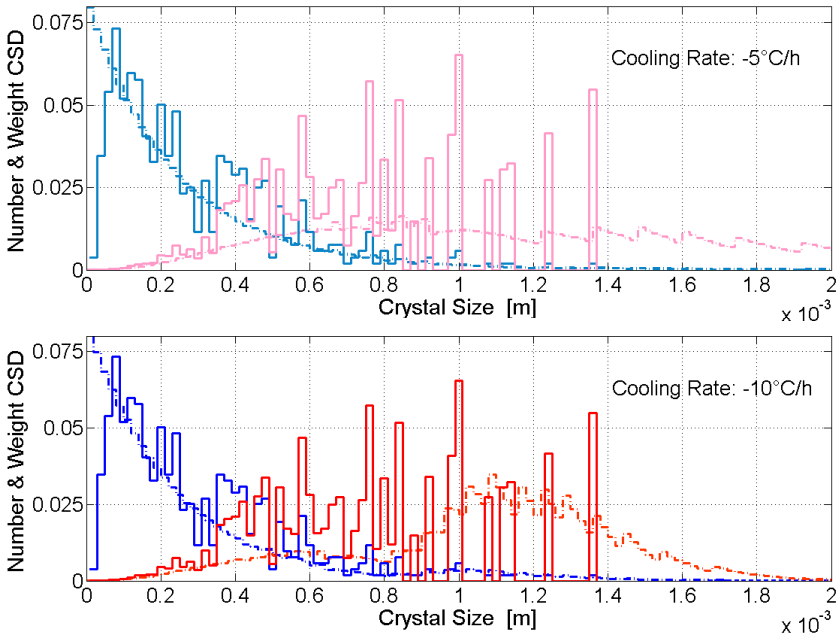
Number & Weight CSD
Cooling Rate: -5°C/h
Crystal Size [m]
x 10^-3
Number & Weight CSD
Cooling Rate: -10°C/h
Crystal Size [m]
x 10^-3

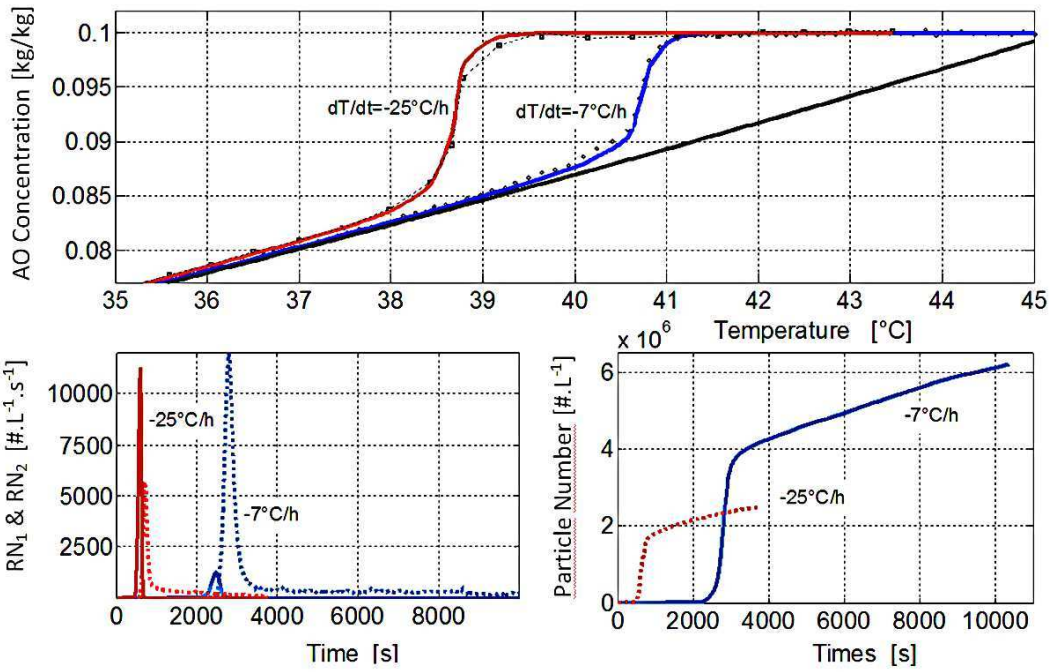
AO Concentration [kg/kg]
dT/dt=-25°C/h
dT/dt=-7°C/h
Temperature [°C]
RN1 & RN2 [#.L-1.s-1]
-25°C/h
-7°C/h
Time [s]
x 10^6
Particle Number [#.L-1]
-7°C/h
-25°C/h
Times [s]

Figures 9 and 10

It is worthy of noting that the *in situ* images provided by the EZ probe (see Fig. 2) tend to confirm the onset of secondary nucleation. Despite the undeniable coarseness of the CSD measurements, the model-predicted CSD displayed in Fig. 9 are rather consistent with the experimental data.

Figure 10 suggests that secondary nucleation occurs more continuously than predicted by the previous model. This point is illustrated in Fig.10b where the rate of nucleation is predicted to be almost constant during the cooling period following the primary nucleation burst. According to the nucleation model (13) and using the parameters given in Table 2, three nucleation periods can roughly be observed during the development of the batch process. The crystallization is initiated by a small and narrow primary nucleation bump. Interestingly, the intensity of this bump appears to depend very significantly on the cooling rate: as one can see on Fig. 10b the maximal nucleation rate, when cooling is performed with dT/dt = -10°C/h, is computed to be 13 times higher than with the cooling rate -5°C/h. During a second period, the particle number increases sharply, during about 300 s for -10°C/h and 600 s when the cooling rate is -5°C/h (see the arrows in Fig.10b). The third period shows a linear increase in the overall particle number: the secondary nucleation rate is almost constant during this period. Actually, the experiments and the simulation results suggest that the CSD is dominated by secondary nucleation mechanisms, these latter mechanisms being obviously influenced by the amount of solid particles present in the suspension.

As for the previous identification procedure, two crystallization regimes are again observed that correspond to the same ranges of cooling rates, but it now turns out to be really difficult to develop an overall crystallization model for regime R_2 that would describe the whole set of experimental CSD data. This is why Table.2 only presents the estimated kinetic parameters obtained for regime R_1.

It is interesting to notice that the PBE simulation “predicts” bigger particles at the end of the batch process than the biggest particles measured using image analysis. If one considers the weight distributions in Figs.9 a and b, it appears that the highest particle sizes predicted by the model exceed 2.5 mm with dT/dt=-5°C/h and 1.8 mm with dT/dt=-10°C/h. Such observation could be expected and, in some way, confirms the validity of the PBE modelling. Indeed, the field of the EZ Probe images is 1.3*1 mm. Consequently, it makes no doubt that particles exceeding about 1mm length are most likely to go over the frame, and therefore to be cut out of the counting procedure (since their real length cannot be measured). Moreover, due to the limited resolution of the imaging probe, particles smaller than 5 μm cannot be “seen”. The

contribution of big and of very small particles is therefore widely underestimated in the computation of the size distribution histograms, and most particles exceeding 1.3 mm are likely to be ignored. The experimental observations are therefore fully consistent with the crystallization kinetic estimation and, in turn, are “corrected” by the simulation model.

Conclusions

The dynamic modelling of the batch cooling solution crystallization of ammonium oxalate in water was developed using population balance equations (PBE). The estimation of nucleation and growth parameters was made possible thanks to ATR FTIR measurements of solute concentration and final CSD data computed from in situ images of the crystallizing suspension. The obtained dynamic PBE model allowed analysing the respective contribution of experimental supersaturation and CSD data to the kinetic characterization of crystallization processes. In particular, the examination of the estimation results was intended to examine the possible contributions and limitations of complementary sensing strategies to the in-depth understanding of the nucleation and growth mechanisms governing industrial batch crystallization processes.

It can firstly be concluded that reliable evaluation and understanding of crystallization kinetics require measurements of both the continuous liquid phase and the solid dispersed phase. Even continuous accurate measurements of the solute concentration (which are not that frequently reported in the open literature) cannot be claimed to allow comprehensive estimation of the set of kinetic parameters involved during crystallization. Through the case-study presented here it appears that the knowledge of the time variations of solute concentration allows, at best, evaluating a combination of parameters of the kinetic laws involved, but not their full separate characterization. CSD data are demonstrated to be essential to resolve the entanglement of the nucleation and growth kinetic parameters (even though the demonstration is not claimed to cover any nucleation and growth kinetic situations.)

Secondly, despite the major restriction outlined above, it is shown that the availability of accurate continuous supersaturation data allows discriminating between possible nucleation mechanisms, even in the absence of CSD measurements. During this study two different crystallization regimes were observed, that depend on the cooling rates. Nucleation phenomena occurring at higher cooling rates appeared to be more

complex than at low cooling rate and modelling the supersaturation measurements strongly suggested to account for prevailing secondary nucleation mechanisms.

Thirdly, thanks to both supersaturation and CSD measurements, a rather detailed analysis of possible simultaneous nucleation and growth phenomena was shown to provide better understanding of the crystallization. Nucleation and growth kinetic parameters were thus estimated and the predictive features of the overall PBE model turned out to be satisfactory.

Finally, as far as the AO/water crystallization system is concerned, it is worth outlining that several interesting features were observed and quantified. The cooling crystallization turns out to be rather complex and raises many theoretical questions. The process is subject to 2 different kinetic regimes which depend on the cooling rate (i.e. the rate of generation of supersaturation.) An intermediate irreproducible regime was also observed to occur between the two previous ones. Such behaviour raises interesting theoretical questions. Kinetic nucleation and growth parameters are proposed to quantify the crystallization kinetics at low cooling rates; in this case secondary nucleation appears to be the prevailing particle generation mechanism.

Appendix A.

The solid concentration $C_s(t)$ is computed after integrating the whole set of particles in suspension at time t. Denoting by dv(L) the volume of one single particle of size L, ϕ_v its volumetric shape factor ($\pi/6$ for spherical crystals) and ρ_S the specific mass of AO, one can write:

$$v(L,t) = \phi_v L(t)^3 \;\Rightarrow\; m(L,t) = \rho_s \phi_v L(t)^3$$

Therefore, after integration of the set of size-distributed particles and referring the PDF (Population Density Function) $\psi(L,t)$ (in $(\#.m^{-1}.s^{-1}).m^{-3}$) to 1 unit volume of suspension:

$$C_s(t) = m_{Total}(t) = \rho_s \phi_s \int_0^{L_{max}} \psi(L,t) L(t)^3 dL$$

Whatever the kinetic expression of the growth rate, one can generally write $G(t)=k_g\, g(\beta(t)) = dL/dt$ where $g(\beta(t))$ represents the effect of supersaturation $\beta(t)$ on the crystal growth rate (e.g. $g=\beta+1$, $g=(\beta+1)^2$) and k_g is the growth rate constant (m/s).

It follows that: $$C_s(t) = \rho_s \phi_s \int_0^{L_{max}} \psi(L,t) L(t)^3 dL = \rho_s \phi_s \int_0^{L_{max}} \psi(L,t) \left[\int_\nu^t G(\tau)\, d\tau \right]^3 dL$$

where $\nu(L,t)$ is the nucleation time of the particles with size L(t).

The PDF is defined as $\psi(L,t) = \dfrac{n(L,t)}{dL} = \dfrac{R_N(t)\,dt}{dL} \Rightarrow \psi(L,t)\,dL = A.n(t)\,dt$, where parameter A is here considered as constant and n ($\beta(t)$) depends on supersaturation only (e.g. $n = \exp\left(\dfrac{-B}{(\ln\beta)^2}\right)$).

The following expression of C_s is obtained where t_{fin} is the final batch time:

$$C_s(t) = A \rho_s \varphi_s \int_0^{t_{fin}} n(\beta(t)) dt \left[\int_\nu^t k_g\, g(\beta(\tau)) d\tau \right]^3 = k_g{}^3 A \rho_s \varphi_s \int_0^{t_{fin}} n(\beta(t)) \left[\int_\nu^t g(\beta(\tau)) d\tau \right]^3 dt$$

$$= k_g{}^3 A\, \rho_s \varphi_s \chi(\beta(t))$$

The goal is to estimate A and k_g from measured concentration profiles, the time functions $\beta(t)$ and $C_s(t)$ are thus derived from fixed experimental data such that the following ratio $\chi(\beta(t))$ is constant:

$$\chi(\beta(t)) = \frac{C_s(t)}{\rho_s \varphi_s \int_0^{t_{fin}} n(\beta(t)) \left[\int_v^t g(\beta(\tau)) d\tau \right]^3 dt} = k_g{}^3 A$$

The product $k_g{}^3 A$ is therefore constant for given nucleation and growth expressions and given experimental solute concentration trajectory C(t). Consequently, measuring C(t) yields $k_g{}^3 A$, and does not allow estimating separately k_g and A.

References

1. Yu LX, Lionberger RA, Raw AS, et al. Applications of process analytical technology to crystallization processes. *Advanced Drug Delivery Reviews*. 2004;56(3):349-369.

2. Wu H, White M, Khan MA. Quality-by-Design (QbD): An integrated process analytical technology (PAT) approach for a dynamic pharmaceutical co-precipitation process characterization and process design space development. *International Journal of Pharmaceutics*. 2011;405(1-2):63-78.

3. Yu Z, Chew J, Chow P, Tan R. Recent Advances in Crystallization control: An Industrial Perspective. *Chemical Engineering Research and Design*. 2007;85(7):893-905.

4. LEUENBERGER H, LANZ M. Pharmaceutical powder technology -- from art to science: the challenge of the FDA's Process Analytical Technology initiative. *Advanced Powder Technology*. 2005;16(1):3-25.

5. Févotte G, Caillet A, Sheibat-Othman N. A population balance model of the solution-mediated phase transition of citric acid. *AIChE Journal*. 2007;53(10):2578-2589.

6. Ono T, Kramer HJM, ter Horst JH, Jansens PJ. Process Modeling of the Polymorphic Transformation of l-Glutamic Acid. *Crystal Growth & Design*. 2004;4(6):1161-1167.

7. Qamar S, Ashfaq A, Angelov I, et al. Numerical solutions of population balance models in preferential crystallization. *Chemical Engineering Science*. 2008;63(5):1342-1352.

8. Oullion M, Puel F, Févotte G, Righini S, Carvin P. Industrial batch crystallization of a plate-like organic product. In situ monitoring and 2D-CSD modelling: Part 1: Experimental study. *Chemical Engineering Science*. 2007;62(3):820-832.

9. Eggers J, Kempkes M, Cornel J, et al. Monitoring size and shape during cooling crystallization of ascorbic acid. *Chemical Engineering Science*. 2009;64(1):163-171.

10. Sarkar D, Doan X, Ying Z, Srinivasan R. In situ particle size estimation for crystallization processes by multivariate image analysis. *Chemical Engineering Science*. 2009;64(1):9-19.

11. Zhou Y, Srinivasan R, Lakshminarayanan S. Critical evaluation of image processing approaches for real-time crystal size measurements. *Computers & Chemical Engineering*. 2009;33(5):1022-1035.

12. Saleeby EG, Lee HW. Solution and analysis for crystallization with agglomeration. *Chemical Engineering Science*. 1994;49(12):1879-1884.

13. Briesen H. Two-dimensional population balance modeling for shape dependent crystal attrition. *Chemical Engineering Science*. 2009;64(4):661-672.

14. Simon LL, Nagy ZK, Hungerbuhler K. Endoscopy-Based in Situ Bulk Video Imaging of Batch Crystallization Processes. *Organic Process Research & Development*. 2009;13(6):1254-1261.

15. Mozina M, Tomazevic D, Leben S, Pernus F, Likar B. Digital imaging as a process analytical technology tool for fluid-bed pellet coating process. *European Journal of Pharmaceutical Sciences*. 2010;41(1):156-162.

16. Nagy ZK, Chew JW, Fujiwara M, Braatz RD. Comparative performance of concentration and temperature controlled batch crystallizations. *Journal of Process Control*. 2008;18(3-4):399-407.

17. Ma DL, Braatz RD. Robust identification and control of batch processes. *Computers & Chemical Engineering*. 2003;27(8-9):1175-1184.

18. Chung SH, Ma DL, Braatz RD. Optimal model-based experimental design in batch crystallization. *Chemometrics and Intelligent Laboratory Systems*. 2000;50(1):83-90.

19. Söhnel O, Mullin JW. Interpretation of crystallization induction periods. *Journal of Colloid and Interface Science*. 1988;123(1):43-50.

20. Kashchiev D, Verdoes D, van Rosmalen GM. Induction time and metastability limit in new phase formation. *Journal of Crystal Growth*. 1991;110(3):373-380.

21. Verdoes D, Kashchiev D, van Rosmalen GM. Determination of nucleation and growth rates from induction times in seeded and unseeded precipitation of calcium carbonate. *Journal of Crystal Growth*. 1992;118(3-4):401-413.

22. Sangwal K. *Additives and Crystallization Processes*. Chichester, UK: John Wiley & Sons, Ltd; 2007. Available at: http://onlinelibrary.wiley.com/book/10.1002/9780470517833 [Accédé Septembre 17, 2010].

23. Sangwal K. Kinetic effects of impurities on the growth of single crystals from solutions. *Journal of Crystal Growth*. 1999;203(1-2):197-212.

24. Sangwal K. Growth kinetics and surface morphology of crystals grown from solutions: Recent observations and their interpretations. *Progress in Crystal Growth and Characterization of Materials*. 1998;36(3):163-248.

25. Sangwal K, Mielniczek-Brzoska E. Effect of cationic impurities on solubility and crystal growth processes of ammonium oxalate monohydrate: Role of formation of metal-oxalate complexes. *Crystal Research and Technology*. 2007;42(6):531-543.

26. Sangwal K, Mielniczek-Brzóska E. Effect of Cr(III) ions on the growth kinetics of ammonium oxalate monohydrate crystals from aqueous solutions. *Journal of Crystal Growth*. 2002;242(3-4):421-434.

27. Sangwal K, Mielniczek-Brzoska E. Effect of Fe(III) ions on the growth kinetics of ammonium oxalate monohydrate crystals from aqueous solutions. *Journal of Crystal Growth*. 2001;233(1-2):343-354.

28. Mielniczek-Brzoska E, Gielzak-Kocwin K, Sangwal K. Effect of Cu(II) ions on the growth of ammonium oxalate monohydrate crystals from aqueous solutions: growth kinetics, segregation coefficient and characterisation of incorporation sites. *Journal of Crystal Growth*. 2000;212(3-4):532-542.

29. Lindenberg C, Mazzotti M. Effect of temperature on the nucleation kinetics of [alpha] l-glutamic acid. *Journal of Crystal Growth*. 2009;311(4):1178-1184.

30. Ramkrishna D. *Population Balances: Theory and Applications to Particulate Systems in Engineering*. Academic Press; 2000.

31. Briesen H. Simulation of crystal size and shape by means of a reduced two-dimensional population balance model. *Chemical Engineering Science*. 2006;61(1):104-112.

32. Sato K, Nagai H, Hasegawa K, et al. Two-dimensional population balance model with breakage of high aspect ratio crystals for batch crystallization. *Chemical Engineering Science*. 2008;63(12):3271-3278.

33. Bajpai RK, Ramkrishna D, Prokop A. A coalescence redispersion model for drop-size distributions in an agitated vessel. *Chemical Engineering Science*. 1976;31(10):913-920.

34. Mersmann A. Crystallization and precipitation. *Chemical Engineering and Processing*. 1999;38(4-6):345-353.

35. Mullin J. Allan S. Myerson, Handbook of Industrial Crystallization (2nd edition), Butterworth-Heinemann (2002) ISBN 0-7506-7012-6 313 pp. *Chemical Engineering Research and Design*. 2004;82(1):116.

36. Chernov AA. Notes on interface growth kinetics 50 years after Burton, Cabrera and Frank. *Journal of Crystal Growth*. 2004;264(4):499-518.

37. Burton WK, Cabrera N, Frank FC. The Growth of Crystals and the Equilibrium Structure of their Surfaces. *Philosophical Transactions of the Royal Society of London. Series A, Mathematical and Physical Sciences*. 1951;243(866):299 -358.

38. Sangwal, K., Zdyb A, Chocyk D, Mielniczek-Brzóska, E. Effect of Supersaturation and Temperature on the Growth Morphology of Ammonium Oxalate Monohydrate Crystals Obtained from Aqueous Solutions. *Crystal Research and Technology*. 1996;31:267-273.

39. Mullin, J.W. *Crystallization, 3rd Ed.*. London (UK): Butterworth-Heinemann,; 1993.

40. Garside, J., Larson, M. Direct observation of secondary nuclei production. *Journal of Crystal Growth*. 1978;43:694-704.

41. Févotte F, Févotte G. A method of characteristics for solving population balance equations (PBE) describing the adsorption of impurities during crystallization processes. *Chemical Engineering Science*. 2010;65(10):3191-3198.

42. Togkalidou T, Fujiwara M, Patel S, Braatz RD. Solute concentration prediction using chemometrics and ATR-FTIR spectroscopy. *Journal of Crystal Growth*. 2001;231(4):534-543.

43. Pöllänen K, Häkkinen A, Reinikainen S, et al. IR spectroscopy together with multivariate data analysis as a process analytical tool for in-line monitoring of crystallization process and solid-state analysis of crystalline product. *Journal of Pharmaceutical and Biomedical Analysis*. 2005;38(2):275-284.

44. Lewiner F, Klein JP, Puel F, Févotte G. On-line ATR FTIR measurement of supersaturation during solution crystallization processes. Calibration and applications on three solute/solvent systems. *Chemical Engineering Science*. 2001;56(6):2069-2084.

45. Scholl J, Bonalumi D, Vicum L, Mazzotti M, Muller M. In Situ Monitoring and Modeling of the Solvent-Mediated Polymorphic Transformation of L-Glutamic Acid. *Crystal Growth & Design*. 2006;6(4):881-891.

46. Gherras N, Févotte G. Comparison between experimental approaches for the experimental determination of metastable zone width: a case study of the batch cooling crystallization of ammonium oxalate in water. *J. Cryst. Growth (Submitted)*. 2011.

47. Févotte G. New perspectives for the on-line monitoring of pharmaceutical crystallization processes using in situ infrared spectroscopy. *International Journal of Pharmaceutics*. 2002;241(2):263-278.

48. Presles B, Debayle J, Févotte G, Pinoli J. Novel image analysis method for in situ monitoring the particle size distribution of batch crystallization processes. *J. Electron. Imaging*. 2010;19(3):031207.

Table.1: Optimal nucleation and growth kinetic parameters: observation of two different crystallization regimes, depending on the cooling rate. The experimental results were not found to be reproducible in the intermediate region (i.e. for -15 °C/h > dT/dt > -25 °C/h). The experimental solute concentration profile was fitted to the simulated one.

```
x=   [112.58868280920512   6.9863  3.6309  1.5202    1.5956];
%
% G= 25.071532639213409*1e-6*sigma
```

(2) Referred to as “Model 2.n” in the text, the simulation results C(t) and RN(t) are displayed in figures 6.

(3) The simulation results C(t) and RN(t) are displayed in figures 7 and 8.

Table.1: Optimal nucleation and growth kinetic parameters: observation of two different crystallization regimes, depending on the cooling rate. The experimental results were not found to be reproducible in the intermediate region (i.e. for -15 °C/h > dT/dt > -25 °C/h). The experimental solute concentration profile was fitted to the simulated one.

Equations:	(8)		(13)			(7)		
Crystallization regime (depending on dT/dt)	A_{hom} ($\#.m^{-3}.s^{-1}$)	B_{hom} (-)	A_{SN}	i	k	k_g ($s.m^{-1}$)	j	Nucleation mechanism
1.1 R_1 (≈) (dT/dt ≤ 15°C/h)	$5.05\ 10^{6}$	$3.83\ 10^{6}$	-	-	0	$2\ 10^{-5}$ (*)	1	RN_1
1.2 R_2 (≈) (separate optimization with dT/dt=30°C/h)	$2.9\ 10^{4}$	$2.78\ 10^{6}$	-	-	0	$2\ 10^{-5}$ (*)	1	RN_1
2.1 R_1 (❄) (dT/dt ≤ 15°C/h)	$5.96\ 10^{7}$	$4.14\ 10^{6}$	$1.4\ 10^{9}$	1.36	1.8	$2.40\ 10^{-5}$	1	$RN_1 + RN_1$
2.2 R_2 (❄) (dT/dt ≥ 25°C/h)	$7.05\ 10^{7}$	$6.98\ 10^{6}$	$1.4\ 10^{9}$	1.36	1.78	$2.70\ 10^{-5}$	1	$RN_1 + RN_1$

(*) The growth rate constant was fixed to $k_g = 2\ 10^{-5}$ m/s such that the final maximum particle size was consistent with real crystals (i.e. between about 1 and 4 mm, depending on the cooling rate)

(≈) Estimations performed using concentration measurements only.

(❄) Estimations performed using both concentration and granulometric data.